JOURNAL OF CATALYSIS **161,** 480–494 (1996)
ARTICLE NO. 0207

Effect of Various Pretreatments on the Structure and Properties of Ruthenium Catalysts

Geoffrey C. Bond,*[,1] Bernard Coq,† Roger Dutartre,† Joaquin Garcia Ruiz,‡ Andrew D. Hooper,* M. Grazia Proietti,‡ M. Concepcion Sanchez Sierra,‡ and Joop C. Slaa*

**Department of Chemistry, Brunel University, Uxbridge UB8 3PH, United Kingdom; †Laboratoire de Matériaux Catalytiques et Catalyse en Chimie Organique, ENSCM, Université de Montpellier, 8 Rue de l'Ecole Normale, 34053 Montpellier Cedex 1, France; and ‡Instituto de Ciencias de Materiales de Aragón, Facultad de Ciencias, CSIC-Universidad de Zaragoza, Pza. S. Francisco s/n, 50009 Zaragoza, Spain*

Received July 28, 1995; revised January 3, 1996; accepted January 31, 1996

The effect of oxidation (623 K) followed by low-temperature reduction (433 K) (O/LTR) on a very highly dispersed 1% Ru/Al_2O_3 catalyst previously reduced at high temperature (753 K) (HTR1) on the hydrogenolysis of ethane ($H_2 : C_2H_6 = 10 : 1$) is to increase the turnover frequency (TOF) at 433 K by a factor of about 200 with respect to that shown after HTR1. Its effect on the hydrogenolysis of 2,2,3,3-tetramethylbutane is also to increase TOF, but in addition the demethylation ($\alpha\gamma$) mode of reaction is suppressed and the extent of deep hydrogenolysis is increased. EXAFS measurements show that the O/LTR procedure causes first migration and coalescence of oxidic species and then formation of aggregates of larger metal particles; these are, however, amorphous to X-rays. The enhancement of TOF is therefore not explicable by an increase in the active area; it is, however, partially or completely negated by a second high-temperature reduction (HTR2). Similar effects are observed with Ru powder. Mathematical modeling of the dependence of the rate of ethane hydrogenolysis on H_2 pressure by a rate expression predicated on the formation of a partially dehydrogenated intermediate indicates that the rate enhancement given by the O/LTR treatment is chiefly due to an increase in the equilibrium constant defining the dehydrogenation; its value and that of K_H, which defines the H_2 chemisorption equilibrium, are both lowered by HTR2. Possible explanations in terms either of surface morphology or of alterations in electronic character are considered.

INTRODUCTION

The central problem in the study of heterogeneous catalysis remains the correlation between the physicochemical structure of the surface and its catalytic behavior. Numerous difficulties attend efforts to forge such connections, which may well be unique to each reaction, or class of reaction; not the least of these difficulties is the suspicion that the surface may restructure in the presence of the reactants in a manner that is conducive to the reaction. However, any information that bears on the dependence of catalytic performance upon surface structure is likely to lead toward a better understanding of heterogeneous catalysis.

In these endeavours, research on hydrocarbon transformations on supported metal catalysts holds pride of place, by reason of the wealth of behavioral characteristics that are available for observation. Such reactions are traditionally regarded as being "structure sensitive," although as has been pointed out (1) this is a concept that needs refinement. Structure sensitivity is a property of a catalytic *system*, that is to say, of the combination of metal and reactants. There is still insufficient information available to formulate the ground rules, but it is clear that a given reaction is not necessarily structure sensitive on all metals. It appears that the effect may be manifested by a dependence of rate on surface geometry, this being the original concept, but it is now often perceived through a variation of rate with particle size, which, through a *presumed* link between particle size and the availability of sites of the necessary sort, is taken to confirm its occurrence.

More subtle but even more significant effects are observed in the measurement of product selectivities, as for example in the hydrogenolysis and skeletal isomerization of linear alkanes on metals. Selectivities are in many ways more suited to the study of structure sensitivity than are rates, because they are often less affected by accidental circumstances, such as poisoning, whether autogenous or caused by impurities. This comparative lack of response to surface cleanliness is in itself informative. Reactions of linear alkanes on certain metals appear to be almost insensitive to factors such as metal particle size and surface cleanliness; thus, for example, platinum (2) and palladium (3) seem to give much the same hydrogenolysis product distributions in a variety of circumstances and, thus, to show a characteristic fingerprint, although isomerization selectivities can vary widely. Any differences between one form of catalyst and another are generally second-order effects. Some other metals, however, afford very variable hydrogenolysis

[1] To whom correspondence should be addressed.

0021-9517/96 $18.00

product distributions; such a metal is ruthenium, and for this reason its catalysis of hydrocarbon transformations has been the subject of intensive study (1, 4–12).

Structure sensitivity is shown even more clearly by branched alkanes containing one or more quaternary atoms which restrict the possible types of species that may be formed initially or limit the extent to which processes of a given type may propagate within a molecule. Thus, for example, 2,2,3,3-tetramethylbutane may form only $\alpha\alpha$-, $\alpha\gamma$-, or $\alpha\delta$-diadsorbed species (8, 9), while 2,2-dimethylbutane (neohexane) may give $\alpha\alpha$, $\alpha\beta$, and $\alpha\gamma$ species: however, $\alpha\beta$ diadsorption is limited to the ethyl group (13). There is much evidence to show that selectivities to products from these alternative routes are structure sensitive, in the sense of both particle size variation (8) and the alteration either of mean ensemble size or the availability of a certain class of surface atom as defined by coordination number (9). With these more complex molecules it is easy to identify probable intermediates differing in structure, although it may be less easy to explain *why* different structures can exist in various circumstances. With linear alkanes, there is no certain means of establishing whether differences in behavior arise from different *species* or from the same species *reacting differently*.

In this paper we focus on the effects produced in the hydrogenolysis of both linear and branched alkanes by the manner in which Ru/Al_2O_3 catalysts are activated. Some years ago it was shown that the activities and product selectivities shown by Ru/TiO_2 catalysts in *n*-butane hydrogenolysis varied very much with the pretreatment applied (4, 5); this was attributed to the effect of the strong metal–support interaction (SMSI) and to the presence of impurities such as Cl^-. To remove the latter and to ensure a non-SMSI state as point of reference, the catalysts were oxidized and then reduced under mild conditions. Various conditions were tried (4), but ultimately oxidation at 623 K (1 h) and overnight reduction at 433 K were adopted as the standard pretreatment to achieve this. This produced catalysts of very high activity, with a propensity to deep hydrogenolysis (i.e., high CH_4 selectivities); this pretreatment, now coded O/LTR, appeared to give high Ru dispersions (12).

It was therefore unexpected to find (12) that with a support such as Al_2O_3, which has no reputation for participating in SMSI, similar effects could be observed. We have recently confirmed and extended these observations with a different set of catalysts made from Cl^--free precursor (6), but with this support the O/LTR treatment leads to dispersions distinctly *lower* than those given by an initial high-temperature reduction (HTR). However, although large particles give higher turnover frequencies (TOFs) than small ones (6), the increase in particle size was not of itself an adequate explanation for the increase in rate, because the behavior characteristic of the O/LTR treatment could be substantially altered by a further HTR, which did not significantly change the particle size. We were therefore led to suggest as possible explanations for the peculiar properties generated by O/LTR either (i) a morphologic factor, e.g., an increase in surface roughness or (ii) an effect due to the presence of unreduced Ru^{x+} ions. Recent observations with supported Rh catalysts (14) and with a number of supported metals of group 10 (15) have established the generality of the phenomenon. This paper develops the investigation of the effect by reporting EXAFS results and a study of the hydrogenolysis of 2,2,3,3-tetramethylbutane on catalysts subjected to O/LTR, and extends the information already available on the hydrogenolysis of the lower linear alkanes (6, 7).

EXPERIMENTAL

Preparation and Pretreatment of Catalysts

Catalysts RuEC1 and RuEC3 were prepared by treating γ-Al_2O_3 (220 m^2g^{-1}, Rhône-Poulenc) with a solution of $Ru(acac)_3$ in toluene for 72 h; after filtration (RuEC1) or evaporation of solvent (RuEC3), precursors were dried *in vacuo*, decomposed in N_2 at 523 K and subsequently reduced in H_2 at respectively 623 and 823 K under conditions that have been fully described before (11). Aliquots of these catalysts (typically ~200 mg) which had been stored in air were reduced *in situ*, according to one of three schedules: HTR1, reduction at 753 K in H_2 for 13 h; O/LTR, air oxidation for 1 h at 623 K, followed by reduction at 433 K for 1 h; HTR2, a repetition of HTR1. These treatments were applied in sequence to the same portion of catalyst, and a series of catalytic measurements were performed after each. Further details of these standard procedures have already appeared (6); variations to them will be mentioned in the text. Composition and other features of the catalysts are given in Table 1.

Ru powder (Johnson Matthey plc) was admixed with nine times its weight of the same γ-Al_2O_3 before use.

TABLE 1

Composition and Chemisorptive Properties of Ru/Al_2O_3 Catalysts

Catalyst	Ru (wt%)	Pretreatment	$(H/Ru)_{irr}$	$(H/Ru)_{tot}$	CO/Ru
RuEC1	0.97	HTR1	0.71	0.88,[a] 0.85[a]	1.31
		O/LTR	0.15	0.19,[b] 0.18,[a] 0.21[a]	—
		HTR2	0.08	0.18,[b] 0.13,[a] 0.17[a]	—
RuEC3	4.0	HTR1	0.19	0.23[b]	0.27
		O/LTR	—	0.083[b]	—
		HTR2	—	0.075[b]	—

[a] Measured at ENSCM, Montpellier.
[b] Measured at Brunel University.

Selective Gas Chemisorption

The double-isotherm method (16) was used at Montpellier for H_2 chemisorption in a static volumetric apparatus; after one of the standard pretreatments, the sample was outgassed at 623 K, and the first isotherm was obtained at 373 K in the range 0–20 kPa. After its completion, the sample was outgassed for 30 min at 373 K and the isotherm determination was repeated. Chemisorption was performed at 373 K rather than at ambient temperature because the time required for equilibration after each H_2 introduction was much shorter (30 min compared with 3–4h). However, on comparing (11) our results for H_2 chemisorption, TEM and EXAFS, we concluded that the difference method (16), which is supposed to measured the "irreversible" H_2 chemisorption, does not give values for dispersion that are compatible with those suggested by the other techniques, and we therefore take the value provided by the first isotherm, viz., $(H/Ru)_{tot}$, for the purpose of calculating TOF values.

EXAFS and XRD

X-ray measurements at the Ru *K*-edge were carried out at the beam-line XAS IV of the storage ring DCI of LURE (Laboratoire pour l'Utilization de la Radiation Electromagnetique) at Orsay (17, 18). A double-crystal Ge (400) monochromator was used, and the storage ring operated at 1.8 GeV with an average current of 150 mA. The experiments were performed at room temperature in the transmission mode, and the samples were mounted in a special chamber which allowed thermal treatments to be performed *in situ*. The EXAFS spectra at the Ru *K*-edge were recorded on samples "as received" (air exposed) and after pretreatments HTR1, O/LTR, and HTR2 described above.

Experimental EXAFS spectra were extracted from the raw spectra using standard techniques (19, 20). They have been analyzed by curve fitting, using for backscattering amplitude and phase shifts for the Ru–Ru contribution values obtained from metallic Ru. The first-shell contribution was extracted by Fourier filtering of the spectra between 0.15 and 0.28 nm. A detailed description of the treatment of the results has already been published (17).

X-ray diffraction measurements were carried at Zaragoza, using a rotating Cu anode as source. The diffracted beam was monochromatized by a graphite crystal, and diffraction patterns were recorded after each of the thermal treatments. At Montpellier further XRD measurements under flowing reactive gases were carried out using a Philips X-ray generator with a Cu anode as X-ray source (40 kV, 30 mA). The sample was supported on a stainless-steel sheet placed inside a dedicated CGR heating chamber; its temperature and collection of the X-ray spectra were monitored with a PC. Use of this special device permitted use of linear heating rates (1 K min^{-1}) in controlled atmospheres. For temperature-programmed oxidation (TPO), $O_2/N_2 = 20/80$ was used, and there were isothermal periods of 40 min at 303 K, for collection of data; a similar procedure was used for temperature-programmed reduction (TPR), but with $H_2/Ar = 5/95$ and 20 K temperature intervals between 353 and 433 K, followed by 50 K intervals to 733 K and finally 753 K.

Alkane Hydrogenolysis

Hydrogenolysis of 2,2,3,3-tetramethylbutane (TeMB, Aldrich, >99%) was performed at atmospheric pressure using high-purity H_2 (>99.99%) in a stainless-steel reactor operated at low conversion (usually <5% except for the more active catalysts) to minimise sequential reactions and to avoid heat and mass transfer limitations. Partial pressures were 1.3 kPa (TeMB) and 99.7 kPa (H_2), and the total flow rate was 10 cm^3 min^{-1}. Analysis was carried out by on-line sampling to a gas chromatograph equipped with a J & W capillary column (30 m × 0.55 mm i.d., DB1 apolar bonded phase). A sample of RuEC1 (~100 mg) was subjected to each of the three pretreatments described above, and then examined at the temperatures specified in Table 3. RuEC3 was reduced in H_2 at 623 K before use. All flow rates were recorded under ambient conditions.

For this reaction the following definitions have been used:

$$\text{conversion (mol\%)} = \left[\left(\sum_1^8 (i/8)C_i\right) \Big/ \left(C_8^0 + \sum_1^8 (i/8)C_i\right)\right] \times 100$$

and

$$\text{selectivity } S_i \text{ to product } i \text{ (mol\%)} = \left[C_i \Big/ \left(\sum_1^8 C_i\right)\right] \times 100,$$

where C_i is the mole percentage in the effluent of the product having i carbon atoms, and C_8^0 is the mole percentage of TeMB in the feed. The depth of hydrogenolysis is defined as the number of fragments produced by one reactant molecule in a single residence, and is expressed as a fragmentation factor ξ which, following Paál and Tétényi (21), is given by

$$\xi = \sum_1^8 C_i \Big/ \sum_1^7 (i/8)C_i.$$

Two types of experiments were carried out with ethane, propane, and *n*-butane.

1. In *thermal cycles*, a sample of catalyst (~200 mg for supported materials) was pretreated according to the schedules described above, and then subjected to a stepwise increase in temperature: each step was about 10 K and a sample was extracted for gas chromatographic analysis toward the end

of each intervening 20-min isothermal period. About ten such steps were usually used. The direction of the temperature flow was then reversed, and a further series of about ten samples were analyzed. A standard gas composition of alkane, 0.071 atm; H_2, 0.714 atm; balance N_2 was used, the flow rates being, in the case of *n*-butane, 140 $cm^3\ min^{-1}$, and with ethane and propane (which are less reactive), 56 $cm^3\ min^{-1}$. By such an experiment it was possible to obtain activation energies based on reactant removal in the increasing and decreasing temperature modes, to observe the effect of temperature on product selectivities, and to assess the extent of deactivation caused by the thermal excursion and the consequential effect on selectivities.

2. In *kinetic measurements* the response of the rate to change in H_2 concentration was determined by use of a reaction pulse method, in which a mixture of the desired composition was allowed to flow over the catalyst for 1 min, toward the end of which time a sample was taken for analysis. H_2 alone was then passed for 19 min, after which another reactant pulse was admitted. More detailed descriptions of this and the thermal cycle method have already been given (6, 7). For ethane hydrogenolysis we report below results obtained at 418 K, using an ethane pressure of 0.071 atm and a total flow rate of 56 $cm^3\ min^{-1}$: H_2 pressures were varied between 0.02 and 0.55 atm, the N_2 flow being varied in sympathy to maintain constant total flow of gas. Deactivation, which was quite severe after each of the HTRs (~50% during the course of the measurements) was corrected for by having frequent recourse to a standard condition (H_2 pressure = 0.16 atm) and adjusting measured rates by an interpolated correction factor (7). No such adjustment was needed after the O/LTR treatment.

For the reactions of the linear alkanes, rates are expressed as mmol $g_{cat}^{-1}\ h^{-1}$, the catalyst weight including that of the support. Selectivity in the reaction of *n*-butane to the product C_j having *j* carbon atoms, S_j, is defined as

$$S_j = 4c_j/(c_1 + 2c_2 + 3c_3),$$

where c_j is the mole fraction of the species C_j in the products. In the reaction of propane

$$S_j = 3c_j/(c_1 + 2c_2).$$

Hydrogenolysis of *n*-butane is supposed to proceed through a chain of adsorbed intermediates C_j^* together with a short-circuit from C_4^* to C_2^* due to fission of the central C–C bond, the fraction of the reaction going thus being given by *F*, the splitting factor (22). First-order rate constants are assigned to each step, and parameters T_j are defined as

$$T_j = k_j'/(k_j' + k_j^*),$$

where k_j' is the rate constant for desorptive reaction of C_j^* and k_j^* is that for its further bond splitting. Steady-state analysis of the reaction network affords equations which in simplified form applicable to low conversion read

$$(S_2/T_2) + S_3 = 1 + F,$$
$$S_3/(1 - F) = T_3.$$

There are insufficient knowns to solve these equations, and we therefore assume that the value of S_2 found in the reaction of propane (defined analogously to S_j above) may be equated to T_2 for *n*-butane reaction under the equivalent conditions. Further explanation of the procedures used will be found in prior publications (6, 7).

The procedure for mathematical modeling of the rate dependence of H_2 concentration has already been described in detail (7), so that only a short summary is needed. Ethane hydrogenolysis is taken to proceed by a classical mechanism involving dehydrogenation by loss of 6-*x* H atoms and formation of the corresponding number of C–Ru bonds. Dissociative H_2 chemisorption occurs in competition, and the slow step is the reaction of the dehydrogenated intermediate with an H atom: removal of C_1^* species as methane is assumed to be fast. This mechanism generates the rate equation termed ES5B (7):

$$r = \frac{k_1 K_A P_A (K_H P_H)^{(n-x)/2}}{[K_A P_A + (K_H P_H)^{(n-x)/2} + (K_H P_H)^{(n+1-x)/2}]^2}$$

where K_A and K_H are equilibrium constants for the dissociative chemisorption of ethane and H_2, respectively, P_A and P_H are their respective pressures, and k_1 is the true rate constant. Optimum values of the constants were obtained by manually changing the value of *x* and then using the Levenberg–Marquardt algorithm (23) to obtain best-fit values of the other constants, until an overall minimum was eventually found.

RESULTS

Selective Gas Chemisorption

Values for $(H/Ru)_{irr}$ and $(H/Ru)_{tot}$ obtained by extrapolating the linear portion of the adsorption isotherms to zero pressure are given in Table 1 for RuEC1 and RuEC3 pretreated in the standard manners.

Transmission Electron Microscopy

RuEC1 treated by HTR1 shows very small particles homogeneously distributed over the support (Figs. 1A and B); they do not give an electron diffraction pattern. Following O/LTR the small particles have disappeared, and there are seen very large patches (50–500 nm) composed of relatively large particles (5–10 nm) (Fig. 1C); they do not, however, show any diffraction pattern of either Ru^0 or RuO_2, and we presume they represent a poorly ordered Ru phase (see below). After HTR2 the micrograph (Fig. 1D)

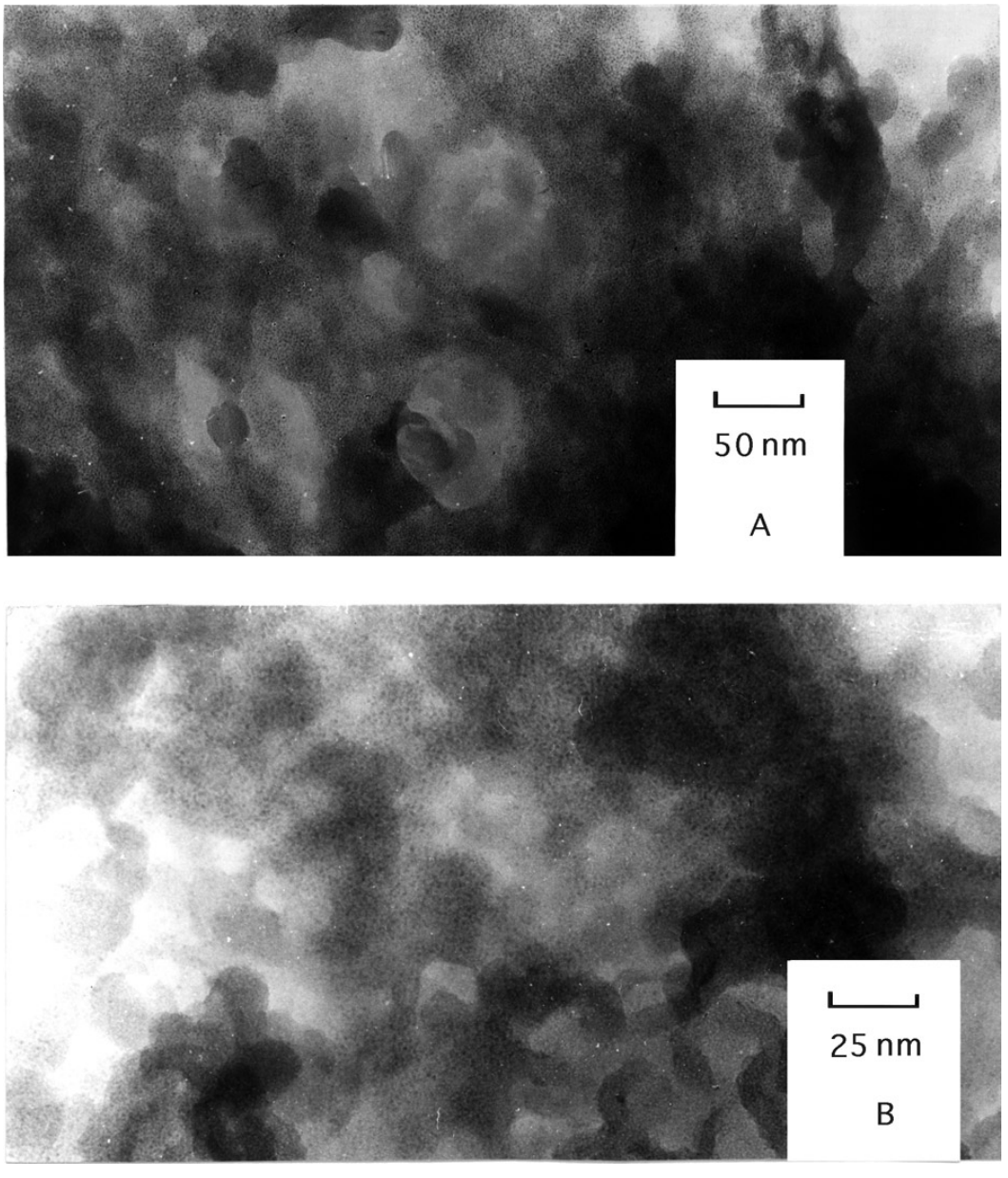

FIG. 1. Transmission electron micrographs of RuEC1 after various pretreatments. (A) HTR1, × 100,000; (B) HTR1, × 200,000; (C) O/LTR, × 100,000; (D) HTR2, × 100,000.

shows little change, but the particles exhibit a very clear microdiffraction pattern of Ru^0, with possible traces of RuO_2. In the case of RuEC3, which before O/LTR showed a wide distribution of particle size (1–10 nm) with some agglomerates, no marked change was observed after O/LTR (6).

EXAFS and XRD

The moduli of the Fourier transform (FT) of the EXAFS spectra for RuEC1 "as received" and after oxidation in air at 623 K are shown in Fig. 2. The former only shows a contribution to oxygen coordination (a peak at 0.16 nm in the FT), indicating that after exposure to air the Ru is totally oxidized, or almost so. The latter shows an analogous oscillatory contribution due to the Ru–O bond, giving rise to a peak in the FT at the some position as before. However, there are also contributions to the EXAFS spectrum at higher frequencies, namely, two peaks appearing in the FT spectrum at 0.27 and 0.33 nm, pointing to an increased ordering of the Ru environment. The overall shape of the FT spectrum of RuEC1 oxidized at 623 K is very similar to that of RuO_2 (24); this treatment appears to induce formation of small particles of crystalline RuO_2 instead of the

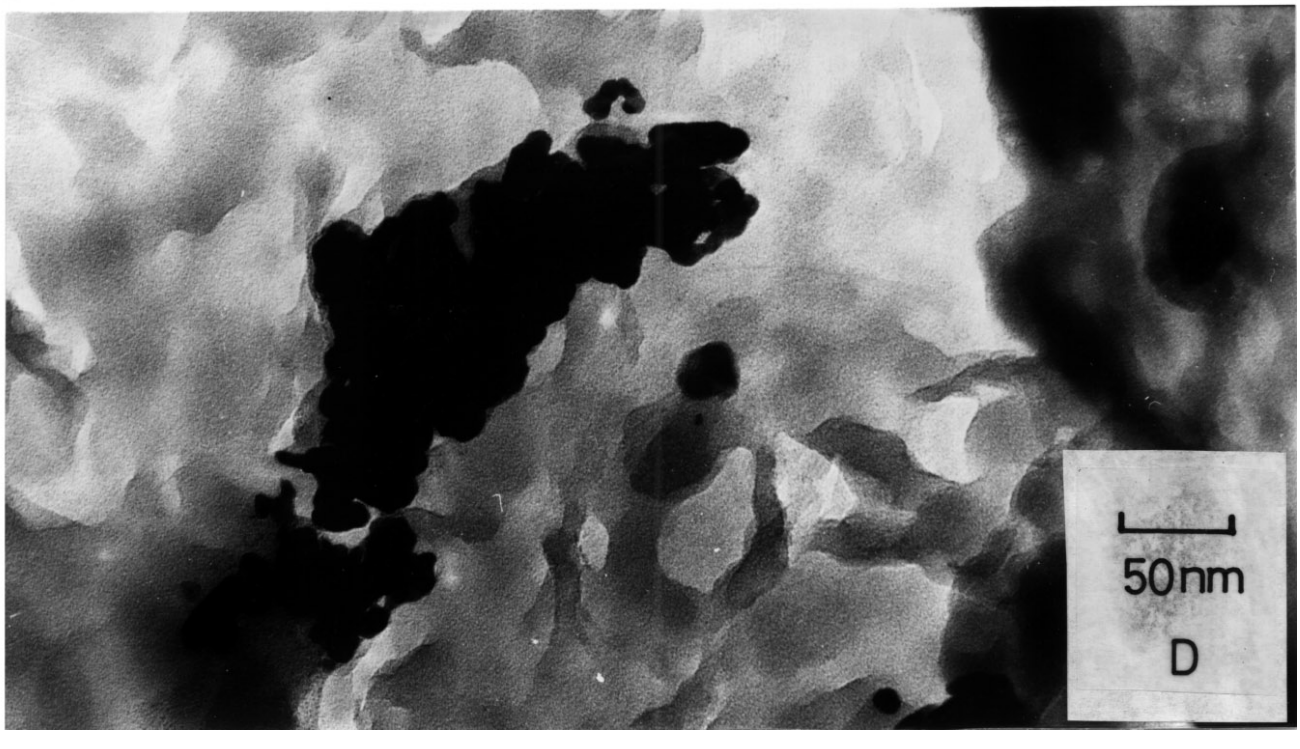

FIG. 1—*Continued*

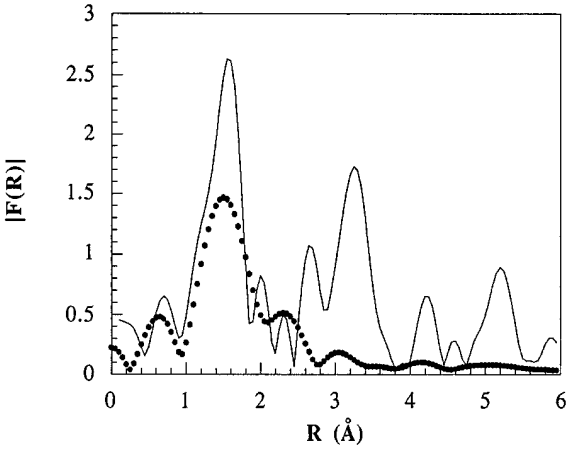

FIG. 2. Fourier transforms of EXAFS spectra of RuEC1 "as received" (open circles) and after oxidation in air at 623 K (continuous line). The peaks at 0.16, 0.27, and 0.33 nm correspond to crystalline RuO_2.

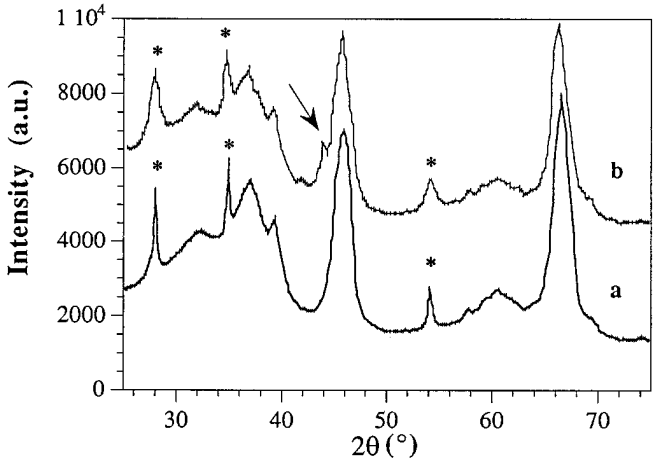

FIG. 4. XRD patterns for RuEC1 (a) and RuEC3 (b) after oxidation at 623 K: reflections due to crystalline RuO_2 (∗) and Ru^0(↓) are superimposed on the Al_2O_3 pattern.

amorphous oxide phase observed in the air-exposed material. Ru cations or RuO_x moieties must therefore become mobile at some temperature between ambient and 623 K, and migrate over the support surface before coalescing into RuO_2 microcrystals.

Similar measurements were made with RuEC3, and the results are shown in Fig. 3. With the "as received" sample, in addition to the peak at 0.16 nm due to Ru–O, there is a peak at 0.33 nm arising from the Ru–Ru distance in crystalline RuO_2; there also appears a further peak at 0.24 nm, which corresponds to a Ru–Ru distance in metallic Ru^0. This shows that, in this less well dispersed catalyst, oxidation under ambient conditions is not complete, and either some metallic Ru particles remain unaltered or at least there is a core of Ru^0 that resists oxidation. The 0.24-nm peak is incompletely resolved from another at 0.27 nm which also is due to a Ru–Ru contribution in RuO_2. Following oxidation at 623 K, the Ru^0–Ru^0 contribution is diminished, and the peaks at 0.16 and 0.33 nm are strengthened, the latter especially, showing that further oxidation and formation of RuO_2 microcrystals have occurred.

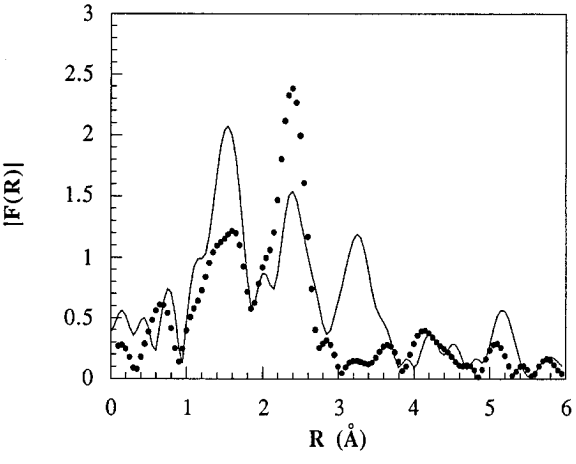

FIG. 3. Fourier transforms of EXAFS spectra of RuEC2 "as received" (open circles) after oxidation in air at 623 K (continuous line). The peak at 0.24 nm is due to Ru^0, and those at 0.16 and 0.33 nm, to crystalline RuO_2.

To corroborate these results, XRD measurements on both RuEC1 and RuEC3 in the high-temperature oxidized state were performed; in the resulting diffraction patterns, shown in Fig. 4, small reflections attributable to crystalline RuO_2 appear in both samples, superimposed upon the Al_2O_3 pattern. However, it is only with the oxidized RuEC3 samples that a peak due to metallic Ru is visible. These XRD results confirm unambiguously those obtained by EXAFS, and the formation of small particles of RuO_2 during oxidation at 623 K is clearly confirmed.

Samples of both RuEC1 and RuEC3 were then subjected to the same pretreatments (HTR1, O/LTR, and HTR2) as were applied before the catalytic and other measurements; the FTs of the resulting EXAFS spectra are shown in Figs. 5 and 6. For both catalysts and after any of the pretreatments, the main peak observed is that at 0.24 nm, due to the Ru–Ru bond. Its intensity is increased after the O/LTR treatment, markedly so in the case of RuEC1, but is only slightly further increased by the HTR2 treatment.

Values for the Ru–Ru interatomic distances, coordination numbers, and Debye–Waller factor differences obtained by best-fit analysis on the EXAFS signal resulting from Fourier filtering in the range 0.15–0.28 nm are summarized in Table 2. The results for samples given the HTR1 treatment agree with those quoted previously (11, 17), and show that after reduction at 723 K the RuEC1 catalyst contains very small Ru clusters comprising no more than 12 atoms. The structural (11) and catalytic (6, 7, 10) properties of this very highly dispersed catalyst have been fully described. The Ru–Ru coordination number for this catalyst

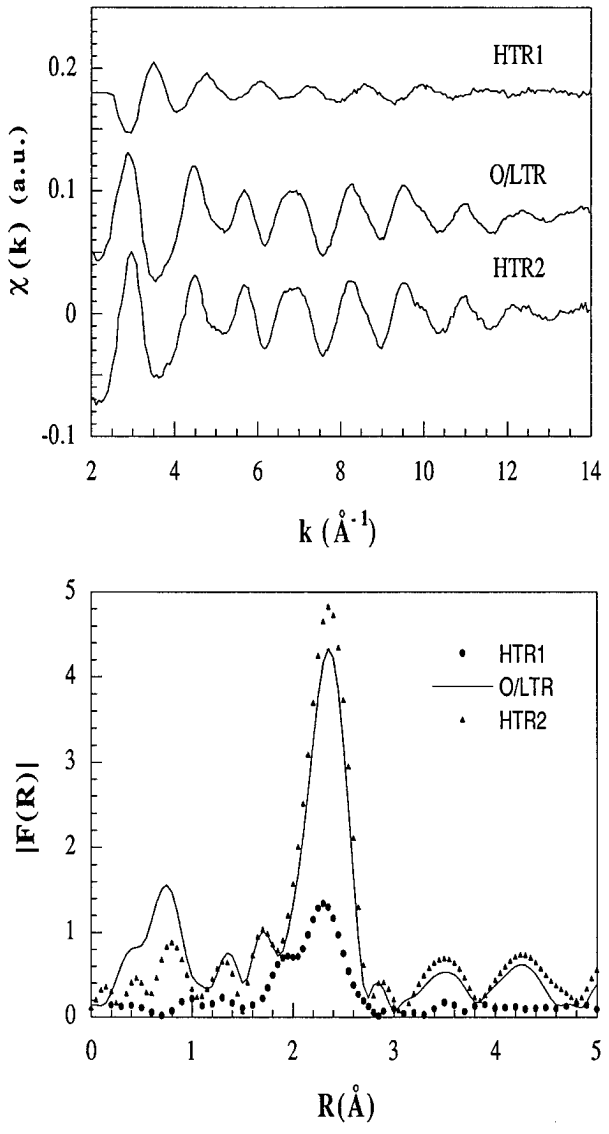

FIG. 5. EXAFS spectra and Fourier transforms for RuEC1 after HTR1, O/LTR, and HTR2 pretreatments.

increases drastically after the O/LTR treatment, reaching a value of 10.6, not far short of the value for bulk Ru, 12. This observation confirms that reduction at 433 K is sufficient to convert RuO_2 to metallic Ru, and that the microcrystals formed in the oxidation lead to quite large Ru particles. A further small increase in coordination number takes place in the HTR2 treatment.

In situ XRD measurements were performed on the TPO of RuEC1; the RuO_2 phase began to appear at about 500 K. Subsequent TPR of the sample oxidized at 623 K showed the disappearance of RuO_2 at 413 K, confirming the conventional TPR profile (11), but at 433 K Ru^0 only showed up as a broad shoulder on the Al_2O_3 peak; this suggests the formation of a highly disordered phase, and confirms the absence of an electron diffraction pattern, noted above.

Performing O/LTR on RuEC3 increases the Ru–Ru coordination number from its already large value of 9.9 after HTR1 to 12; some further increase in particle size has therefore occurred, but no further change is recognisable following HTR2. The derived coordination numbers are in an exact inverse correlation to the $(H/Ru)_{tot}$ values (Table 1), and the mutual support that these measurements exhibit is very gratifying. The large Debye–Waller factors found for RuEC1 following HTR1 are characteristic of systems having a high degree of thermal or structural disorder, and their values run inversely as the coordination number.

Hydrogenolysis of 2,2,3,3-Tetramethylbutane

Results obtained for this reaction on RuEC1 at three temperatures after each of the three standard treatments are compared in Table 3 with those for RuEC3 reactivated at 623 K under H_2. For RuEC1 after HTR1 at the lowest

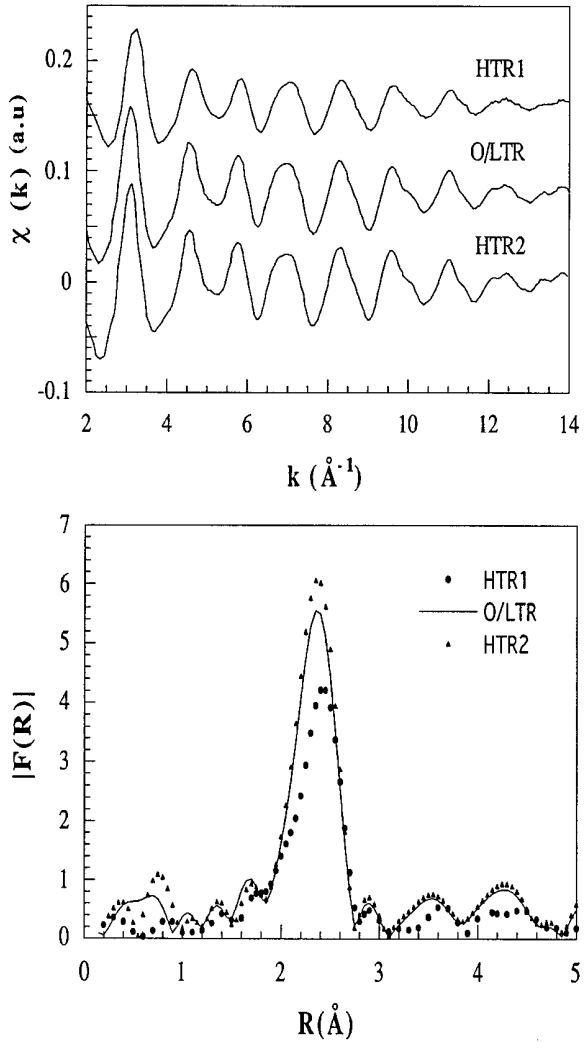

FIG. 6. EXAFS spectra and Fourier transforms of RuEC3 after various pretreatments.

TABLE 2

Best-Fit Parameters Obtained for the First-Shell Contribution for RuEC1 and RuEC3 after Various Treatments

Catalyst	Treatment	Species	N^a	R^b (nm)	$\Delta\sigma^{2\,c}$ ($\times 10^{-5}$/nm^2)
RuEC1	HTR1	Ru^0	3.8	0.260	3.0
		$Ru^{\delta+}$	0.5	0.199	2.0
		O	0.3	0.201	2.0
	O/LTR	Ru^0	10.6	0.268	1.8
	HTR2	Ru^0	11.2	0.268	1.4
RuEC3	HTR1	Ru^0	9.9	0.266	1.8
	O/LTR	Ru^0	12.0	0.267	1.1
	HTR2	Ru^0	12.0	0.267	0.6

[a] Coordination number.
[b] Distance from the absorber.
[c] Difference in Debye–Waller factors between catalysts and reference compounds.

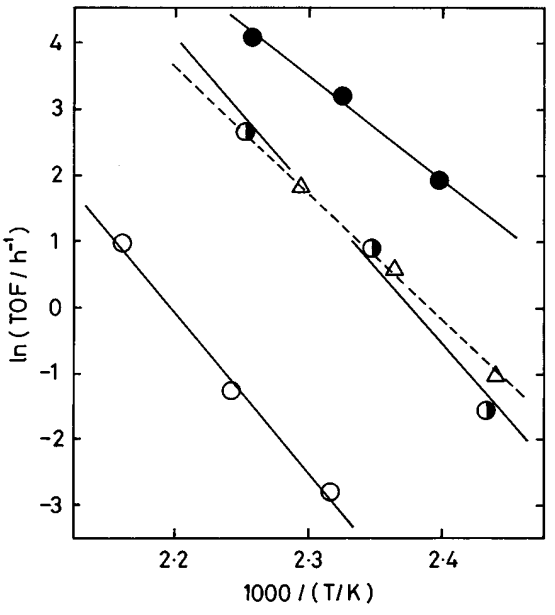

FIG. 7. Arrhenius plots for TOFs of hydrogenolysis of 2,2,3,3-tetramethylbutane over RuEC1 pretreated with HTR1 (○), O/LTR (●), and HTR2 (◐) and over RuEC3 reduced at 623 K (△).

temperature, about three quarters of the reacting molecules undergo terminal C–C bond fission, giving methane + 2,2,3-trimethylbutane (TrMB) ($\alpha\gamma$ mode), and only about one quarter break in the center to give isobutane ($\alpha\delta$ mode). There is no detectable excess hydrogenolysis except at the highest temperature, and values of the fragmentation factor ξ are close to 2. This behavior is characteristic of very well dispersed Ru/Al_2O_3 catalysts (8). It is also noticeable that the mode of reaction shifts toward central bond breaking as the temperature rises, hydrogenolysis through the $\alpha\delta$-diadsorbed species having the higher activation energy (8). Detailed results for the kinetics of the reaction on this catalyst have been presented previously (10).

The O/LTR treatment produces a dramatic change in rate, TOF, and product selectivities (Table 3, Fig. 7). At 430 K the conversion is increased by a factor of about 100 and the TOF by a larger factor of 500 because of the loss of surface area (see Table 1). The reaction pathway changes to predominantly the $\alpha\delta$ mode, but the most noteworthy feature is the much greater amount of deep hydrogenolysis, signalled by the appearance of excess methane and of linear C_2 to C_6 fragments, and values of ξ much in excess of 2. Ethane and propane are most probably formed from adsorbed isobutyl radicals. The apparent activation energy also decreases substantially (Table 3). This change in behavior is partly attributable to the increase in particle size

TABLE 3

Kinetic Parameters and Product Selectivities for Hydrogenolysis of 2,2,3,3-Tetramethylbutane (TrMB) on Ru/Al_2O_3 Catalysts

Catalyst	Treatment	T (K)	Conversion (%)	Product selectivity (mol%)					ξ	E (kJ mol^{-1})	10^3 TOF (s^{-1})
				C_1	C_{2-3}	i-C_4	C_{4-6}	TrMB			
RuEC1	HTR1	432	0.07	39.0	—	23.0	—	38.0	2.01		
		446	0.35	37.2	—	27.4	—	35.4	2.02	201	0.17
		463	1.36	37.8	0.6	32.1	2.8	26.7	2.10		
RuEC1	O/LTR	417	4.0	38.9	11.7	38.2	4.2	5.9	2.72		
		430	14.0	49.6	17.8	26.3	4.3	1.9	3.37	129	84
		443	34.8	62.1	22.4	12.1	2.95	0.4	4.38		
RuEC1	HTR2	411	0.083	21.0	—	79.0	—	—	2.37		
		426	0.99	25.8	8.9	58.7	1.7	4.9	2.43	191	13
		444	5.47	44.6	17.4	34.4	2.1	1.5	3.24		
RuEC3		410	0.47	14.4	2.1	76.2	—	7.2	2.12		
		423	2.29	20.7	6.5	66.6	1.9	4.3	2.32	160	13
		436	8.32	32.7	11.1	50.9	3.0	2.2	2.70		

(Table 1), since with RuEC3, which has a similar dispersion, the reaction also goes chiefly by the $\alpha\delta$ mode (Table 3); the difference lies in the deeper hydrogenolysis that RuEC1 shows after the O/LTR treatment, this having the effect of lowering the isobutane selectivity by one-half.

A further high-temperature reduction (HTR2) decreases the rate more than 10-fold at about 430 K, and the TOF by a factor of 7 (Table 3, Fig. 7). This treatment, which has led to a further small loss of area (Table 1), affords a catalyst which in terms of both TOF and selectivities closely resembles RuEC3 (Fig. 7, Table 3), although the dispersion of the latter is somewhat greater. It is evident that the O/LTR has created a surface that is exceptionally active in deep hydrogenolysis and that the activity can be negated by a high-temperature reduction.

Hydrogenolysis of Linear Alkanes

It is now of interest to enquire whether effects related to those described above are shown by simple linear alkanes and whether analogous behavior is shown by a Ru powder of low dispersion, where there is little chance of further particle growth during O/LTR.

Table 4 gives the Arrhenius parameters, rates, and TOFs for ethane hydrogenolysis on RuEC1 after each of the three standard treatments, with a 10 : 1 H_2 : ethane ratio; Fig. 8 shows Arrhenius plots for the decreasing temperature stages. Once again the O/LTR treatment gives a marked increase in activity, which is greatly diminished by HTR2. Similar results have previously been obtained with propane and *n*-butane (6), so it is certain that the rate and TOF changes are in no way dependent on the alkane structure. There was little or no deactivation with any of the samples during thermal cycling.

The effect of varying H_2 pressure on the ethane hydrogenolysis rate was investigated with RuEC1 at two temperatures after each pretreatment; results obtained at 418 K are shown in Fig. 9. Rates after the HTRs were very similar except at the lower H_2 pressure used, and the expected maxima did not fall within the accessible H_2 pressure range. The great increase in rate effected by the O/LTR is again apparent, and the rate maximum has moved into the range of measurement (~0.04 atm H_2). There were very great differences between the fastest and slowest rates measured, especially after the HTRs (~×500 after HTR2), the power rate law orders in H_2 being $\simeq -2$: for this reason we present the results as log–log plots (Fig. 9). This figure also illustrates the quality of the fits obtained when the results are modelled by the rate expression ES5B; the computed best-fit constants are shown in Table 5. Those for the O/LTR-treated samples are probably the most reliable, as experience with other systems (7) has shown that the existence of a rate maximum greatly helps the fitting process. However, this rate expression provides a very satisfactory model for the variation of rate with H_2 pressure in all three cases. To illustrate the point, after the O/LTR treatment, observed and computed rates at 0.55 atm H_2 pressure are respectively 0.16 and 0.13 mmol g_{cat}^{-1} h^{-1}. Values of k_1 and K_A increase with temperature, while K_H scarcely changes. As noted above, substantial activity loss occurred during measurements with the HTR-treated samples.

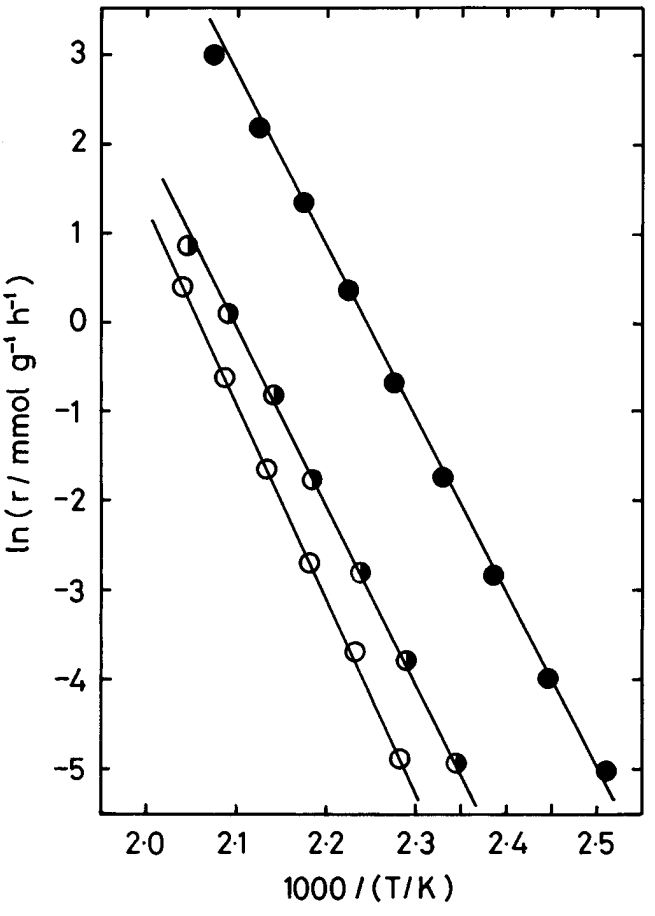

FIG. 8. Arrhenius plots for rates of ethane hydrogenolysis over RuEC1 pretreated with HTR1 (○), O/LTR (●), and HTR2(◐).

Hydrogenolysis of propane and of *n*-butane has been followed on a Ru powder catalyst subjected to the standard

TABLE 4

Kinetic Parameters for Ethane Hydrogenolysis on Ru/Al_2O_3 (RuEC1) after Various Pretreatments[a]

Pretreatment	Temperature range (K)	E (kJ mol^{-1})	ln A^b	Rate^b r	10^3 TOF (s^{-1})
HTR1	490–438	179	44.47	0.485	0.015
O/LTR	482–398	162	43.70	29.3	4.33
HTR2	489–427	163	40.99	1.60	0.25

[a] Results obtained in decreasing temperature stage. Rate and TOF at 433 K.

[b] Rate r and A in mmol g_{cat}^{-1} h^{-1}.

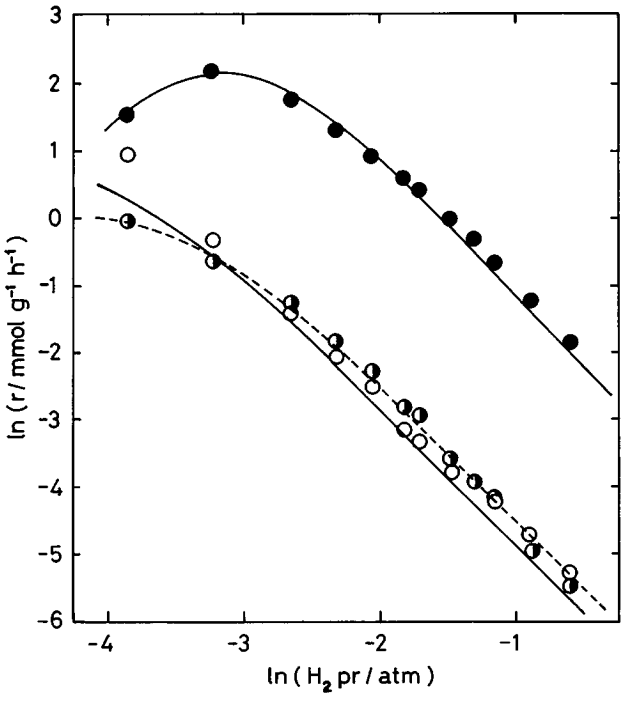

FIG. 9. Log–log plots showing variations in the rate of ethane hydrogenolysis with H_2 pressure on RuEC1 variously pretreated. Experimental points (symbols as in Fig. 8) and lines calculated using the constants for the rate expression ES5B shown in Table 5.

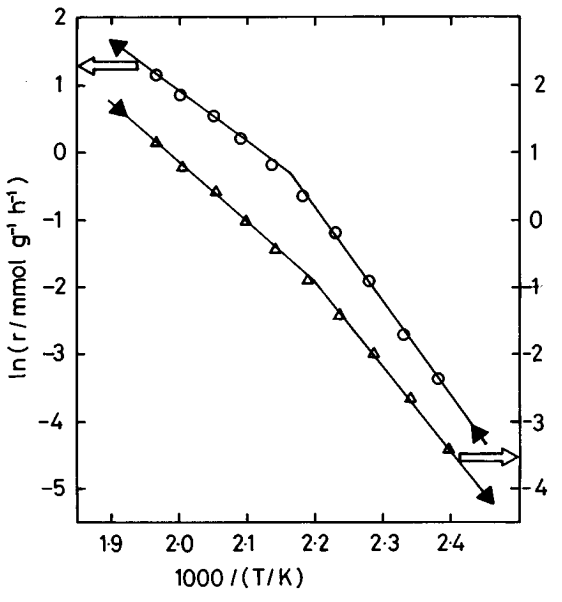

FIG. 10. Arrhenius plots for *n*-butane hydrogenolysis on Ru powder: O, increasing temperature; △, decreasing temperature.

treatments; no attempt was made to look for changes in surface area. Arrhenius plots obtained by stepwise increasing and decreasing temperature ramps, as described above, showed two linear parts (see Fig. 10 for examples) except where too small a temperature range was used (reaction of C_3H_8 after HTR2). Ru/Al_2O_3 catalysts never showed this behaviour under any conditions, although it has been observed with EUROPT-1 ($6\%Pt/SiO_2$) (2). Arrhenius parameters derived from both slopes are shown as compensation effect plots in Fig. 11; while for both reactions the points obtained after the HTRs lie about the same lines, those found after O/LTR lie on parallel lines that are distinctly

TABLE 5

Best-Fit Constants for Equation ES5B Applied to Hydrogenolysis of Alkanes at 418 K on RuEC1 Variously Pretreated

Alkane	Pretreatment	k_1[a]	K_A	K_H	a[b]	Remarks
C_2H_6	HTR1	28.9	0.60	17.6	1.85	—
	O/LTR	71.1	13.5	15.9	1.76	—
	HTR2	13.0	0.40	8.0	1.91	—
C_3H_8	HTR1	80.0	17.1	24.8	2.34	—
	O/LTR	113	75.2	8.0	1.1	Extrap.[c]
	HTR2	12.1	5.6	4.2	1.4	Extrap.[c]
n-C_4H_{10}	HTR1	111	36.7	26.9	1.38	—
	O/LTR	90.9	39.6	3.2	1.2	Interp.[d]
	HTR2	9.25	4.4	1.8	1.2	Interp.[d]

[a] k_1 is still expressed per g_{cat}.

[b] a is the number of H_2 molecules lost in converting the alkane into the reactive form.

[c] Extrapolated.

[d] Interpolated [see (7)].

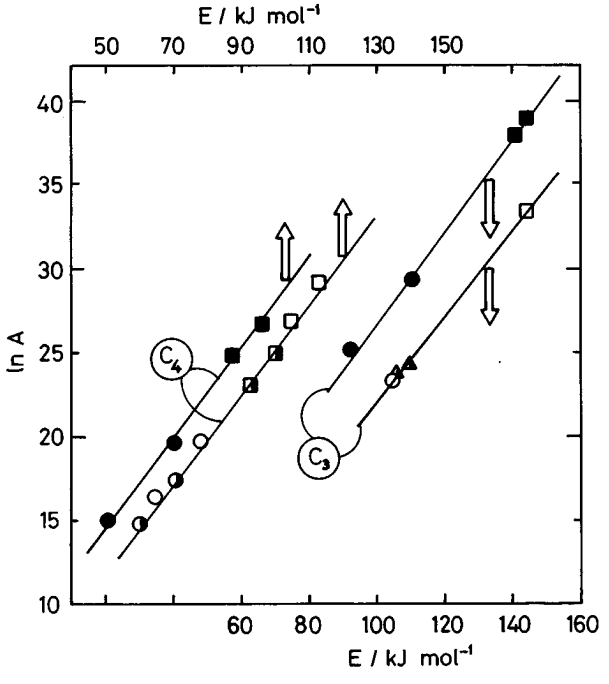

FIG. 11. Arrhenius parameters for hydrogenolysis of propane and of *n*-butane on Ru powder shown as a compensation plot. Circles, high-temperature values; squares, low-temperature values; triangles, media values; open points, HTR1; filled points, O/LTR; half-filled points, HTR2.

TABLE 6

Effect of Pretreatment on TOF or Rate for Hydrogenolysis of Alkanes[a]

Catalyst	Alkane	TOF or rate after pretreatment		
		HTR1	O/LTR	HTR2
RuEC1	C_2H_6	0.015	4.33	0.25
	C_3H_8	0.62	59.3	5.1
	n-C_4H_{10}	9.8	180	48.8
RuEC3	C_3H_8	19.2	423	22.5
	n-C_4H_{10}	100	844	165
Ru powder	C_3H_8	0.012	3.7	0.030
	n-C_4H_{10}	0.95	17.6	0.75

[a] For supported catalysts, values quoted are 10^3 TOF (s^{-1}) at 433 K for linear alkanes and 430 K for TeMB. For Ru powder, values are for rates (mmol g_{Ru}^{-1} h^{-1}) at 433 K.

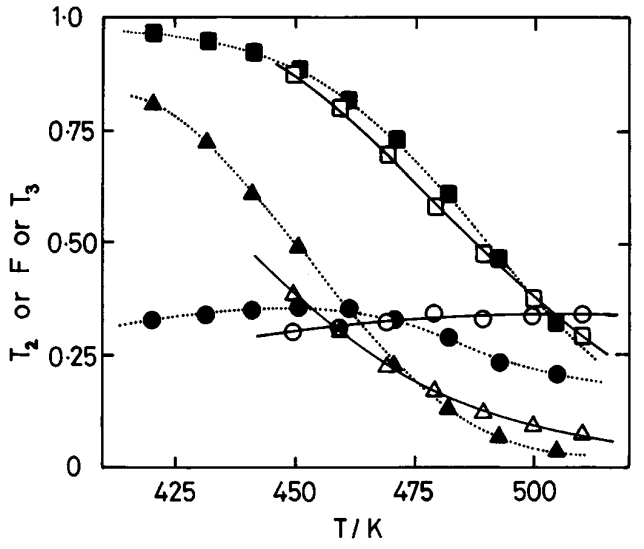

FIG. 12. Temperature dependence of selectivity parameters for the hydrogenolysis of propane and of n-butane over Ru powder: squares, T_2 from propane; triangles, T_3; circles, F. Open symbols, O/LTR; filled symbols, HTR2.

higher. This correlates with the activity changes at 433 K. For n-butane, O/LTR increases the rate over that given by HTR1 by a factor of about 20, while for propane the corresponding factor is much larger (~300); most of the increased activity is lost after HTR2 (Table 6). The change in activity at 433 K between the increasing and decreasing temperature stages was much more evident after the O/LTR treatment, in contrast to the behavior of ethane [and other linear alkanes (6, 7)] on RuEC1. It may also be deduced from Fig. 11 that, while propane is much less reactive than n-butane on catalysts subjected to a HTR, this difference is less after O/LTR. We cannot confidently express rates for Ru powder as TOFs, but using the value of H/Ru = 2.5×10^{-4} (11) they appear to be of the same order of magnitude as for RuEC3 for HTR-treated samples.

Values of S_2, which for the propane reaction are the same as T_2, decrease smoothly with increasing temperature; the manner of the decrease (Fig. 12) is about the same for all three catalysts, values being determined solely by the temperature and not the conversion. The marked differences in activity effected by the pretreatments and the consequent need to use different temperature ranges mean that only a restricted comparison can be made between selectivity parameters for the n-butane reaction, but as Fig. 12 shows, the values of F at conversions of less than 5% are temperature independent and in the range 0.30–0.35 after O/LTR and HTR2.

DISCUSSION

Catalyst Structures

In the "as received" state, that is, after a preliminary reduction and storage in air at ambient temperature, RuEC1 has been shown by TPR and EXAFS to contain fully oxidised Ru species: they do not however exhibit the characteristics of crystalline RuO_2, and are probably best regarded as small clusters of Ru^{4+} and O^{2-} ions having the 12 or so Ru ions that will after reduction constitute the very small Ru^0 particles observed in TEM (11) and EXAFS (17). Oxidation at 623 K mobilises these ions and causes aggregation into RuO_2 microcrystals (Scheme 1). Recalling that RuO_4 is a volatile covalent compound, the formation of which is incidentally not observed, we may suppose that the mobile species may be, for example, RuO_3 entities which hop from one O^{2-} ion to another until they meet and merge with an incipient RuO_2 crystallite which then grows to considerable size. It is noteworthy that according to the TEM results (Figs. 1C and D) the larger Ru^0 particles formed by reduction after oxidation (i.e., by O/LTR) are themselves aggregated. We therefore think that after the oxidation step the RuO_2 is present in patches on the support, and that these fragment on LTR due to the change in lattice parameter, forming large but highly disordered Ru^0 particles (Scheme 1). A further slight increase in particle size occurs during the second HTR (Table 1). Previous EXAFS studies of very small Ru particles on Al_2O_3, prepared either from $Ru(acac)_3$ (26) or from $Ru_3(CO)_{12}$ (27), have afforded results in good agreement with those reported above.

The situation regarding RuEC3 is slightly more difficult, because the particle size distribution of the "as received" catalyst as seen by TEM is clearly bimodal (11), and after HTR1 the mean Ru^0 coordination number given by EXAFS is 9.9. This complicates the interpretation of catalytic behavior, but because large Ru^0 particles exhibit higher values of TOF than small ones for hydrogenolysis reactions, for reasons to be discussed further below, it is they that will contribute most to the observed reaction. The EXAFS and XRD [and TPR (11)] results are consistent with the idea

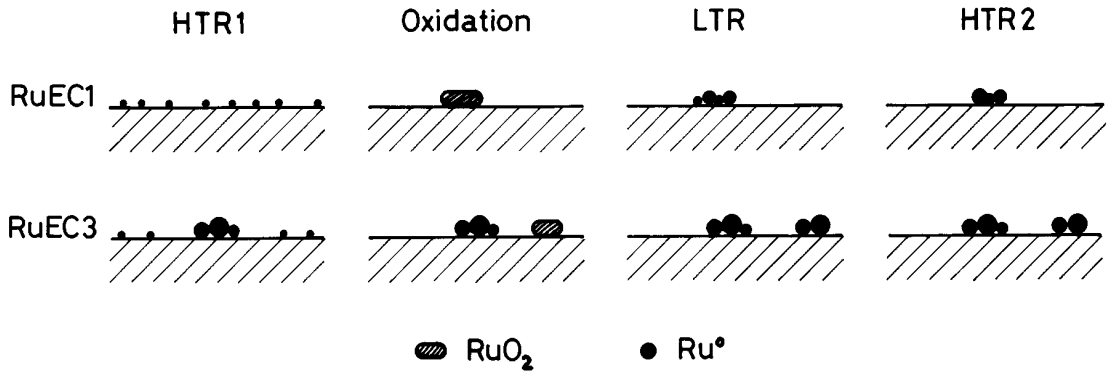

SCHEME 1

that the smaller particles are (as with RuEC1) in an oxidised state in the "as received" material, that they reorganize during oxidation as they do in RuEC1, but that the larger particle fraction remains more or less unchanged apart perhaps from suffering superficial oxidation. After LTR, therefore, we have a mixture of large particles formed by two routes (Scheme 1), the mean dispersion being 8% (Table 1) and the coordination number being indistinguishable from that of bulk Ru (Table 2). HTR2 causes no further change in either of these quantities.

The changes resulting from the O/LTR treatment show a qualitative resemblance to those reported by Kalakkad *et al*. (14) using Rh/SiO_2 and by Gao and Schmidt (15) who used Ru/SiO_2 and other SiO_2-supported metals. In view of the differences in metal, support, and conditions of oxidation and reduction, a precise comparison with our work cannot be made, but it is likely that the breakup of very large RuO_2 particles on SiO_2, seen by TEM to occur as a consequence of reduction (15), may simulate what occurs at the surface of Ru powder during O/LTR.

Effect of Pretreatments on Alkane Hydrogenolysis

We have previously shown in respect of the hydrogenolysis of propane and of *n*-butane on RuEC1 pretreated as described above that the variations in activity observed using a 10-fold excess of H_2 (6) may be traced to differences in the constants of the rate expression ES5B (1). Computational refinement of the results for ethane allows us to compare their values for the three alkanes at 418 K (Table 5), from which certain trends become evident.

1. The O/LTR treatment increases k_1 and K_A to extents that decrease with increasing chain length; it decreases K_H to an extent that increases with chain length. Values of a become slightly lower (a = number of H_2 molecules lost by the alkane).

2. HTR2 causes k_1 and K_A to decrease very markedly with all three alkanes; K_H is further lowered by a factor of about 2 in each case, and a is little changed.

More limited experiments with RuEC3 using *n*-butane have shown that the greater rate shown with a 10-fold excess of H_2 after HTR1, compared with that of RuEC1 (6), stems only partly from a twofold increase in k_1 but mainly from the threefold increase in K_A; K_H is not much altered (1). Thus, reaction on the larger Ru particles present in RuEC3 is facilitated by a greater degree of dehydrogenation of the chemisorbed alkane to the reactive form. Propane behaves similarly. It must be stressed that *there is no direct correlation between the true rate constant k_1 and either rate or TOF*. This conclusion may be illustrated by reference to the results for ethane shown in Tables 4 and 5; similar behavior is shown by propane and *n*-butane, but in these cases the rates after O/LTR are some 20 times faster than after HTR1 at 433 K (6), although k_1 values at 418 K are of similar magnitude (Table 5).

What is particularly noticeable with the hydrogenolysis of ethane on RuEC1 is the much greater stability of the catalyst after O/LTR than after either of the HTRs. The difference is not so clearly apparent in the thermal cycling experiments, but during measurement of the H_2 kinetics, where low H_2/ethane ratios were sometimes used, the residual activity at the end was only about 50% of the initial activity at 418 K following HTRs, while after O/LTR no deactivation whatsoever occurred. It is tempting to associate this very marked effect of pretreatment with the changing values of K_A (Table 5). If deactivation is caused, as has been speculated (25), by the formation of overdehydrogenated species which are unreactive by reason of the greater number of C–M bonds they possess, then such excess dehydrogenation would deplete the concentration of reactive species and a smaller value of K_A would result. We may conclude from the high value of K_A and the absence of deactivation that overdehydrogenation does not occur to any extent with O/LTR-treated Ru/Al_2O_3.

It is of interest to find that qualitatively the same changes in activity with pretreatment occur with the presumably large particles present in Ru powder as are found with Ru/Al_2O_3 catalysts (Table 6). In this case there can be no

mechanism for the aggregation or growth of particles during oxidation, and it is probable that they suffer only superficial oxidation at 623 K. As mentioned above, LTR may then generate smaller crystallites attached to the original surface, so that the much faster rates observed are not necessarily due to higher TOFs. Rates after HTR2 are similar to those found after HTR1 (Table 6), so we may conclude that the particles are sintered back to their original form. If such smaller particles are formed, they must still be large by reference to those found in Al_2O_3-supported catalysts, because, as Fig. 12 shows, the manner in which selectivity parameters change with temperature is not greatly altered. The high values of F and T_3 that characterise the very small Ru particles in RuEC1 after HTR1 are not observed, and the sensitive variations of T_2 and T_3 with temperature epitomise large-particle behavior.

The O/LTR procedure drastically changes the rate and mode of hydrogenolysis of TeMB (Table 3): the rate is much increased, the apparent activation energy is lowered, the $\alpha\gamma$ reaction mode is suppressed, and deeper hydrogenolysis occurs. The selectivity changes are in part accounted for by the increase in particle size (8), but as with the linear alkanes (7), another factor must be at work, because the excessive formation of C_1–C_3 products is not found after the HTR2 treatment (which does not alter the mean particle size) nor with RuEC3 (which has about the same dispersion, Table 1). The special character imparted by the O/LTR treatment thus enhances TOF more than six times and gives [as with linear alkanes (6)] greater fragmentation of the reactant.

We have noted above that application of O/LTR to RuEC1 leads to a lowering of K_H (Table 5), the same being the case with RuEC3 [e.g., at 397–400 K, K_H decreased from 23.0 to 6.2 (7)]; in other words, the coverage of the surface by H atoms θ_H at a given H_2 pressure is reduced. *The values of K_H and θ_H thus depend on the form of the pretreatment and not on the particle size that it generates*. Now with RuEC1 the rate of the $\alpha\gamma$ mode (resulting in demethylation) relative to that of the $\alpha\delta$ mode (which gives isobutane) decreases with decreasing H_2 pressure, so that we may associate both the change of mode and the increase in deep hydrogenolysis with a smaller θ_H; from this it is deduced (10) that both the $\alpha\delta$ mode and multiple fragmentation proceed through more highly dehydrogenated intermediates than does the $\alpha\gamma$ mode. It is satisfying to find parallel effects with TeMB and the linear alkanes, originating in the change in strength of H_2 chemisorption; because of the very different structures of the reactant molecules, we cannot however correlate the shift from $\alpha\gamma$ to $\alpha\delta$ fission modes in TeMB with the decrease that O/LTR causes in the splitting parameter F relating to the linear alkanes.

Origins of Changes in Catalytic Behavior due to O/LTR

We have now established that part of the catalytic effects induced by the O/LTR treatment can be attributed to an increase in mean particle size, but there is clearly an additional effect on TOFs and on product selectivities, as has been remarked upon by others working with related systems (14, 15). This extra effect is substantially cancelled by HTR2; where there is little if any further increase in particle size, similar rates or TOFs are found after HTR1 and HTR2 (e.g., with RuEC3). The recognition that particle size effects and the extra "O/LTR" effect must be traceable to kinetic and thermodynamic terms in the governing rate expression does not, however, constitute an explanation of what is occurring. We shall need ultimately to find logical bases for the reported [(7) and Table 6] changes in these terms, relating them to the conventional geometrical/electronic properties of the Ru particles.

By tradition one first seeks explanations based on geometrical differences, that is, in terms of the types of exposed crystallographic planes and their extents. From the literature it is possible to conclude that the strength of hydrogen chemisorption (28) and the tendency of chemisorbed alkane to dehydrogenate might be plane sensitive. LTR of oxidic species or oxidised surfaces may well produce more open and defective structures than does HTR (15); the possibility that the absence of extended low-index planes militates against the formation of excessively dehydrogenated species has some experimental justification (29). However, two of us have speculated (7) that the unusual characteristics of the very highly dispersed Ru particles present in RuEC1 after HTR1 are associated with the presence of Ru^{x+} ions detected in EXAFS (17, 26) and that these impart an electron-deficient character to the metal clusters. The lower reduction temperature used in the O/LTR procedure might result in a higher proportion of Ru^{x+} ions, which could be removed by HTR2, and hence be the cause of the activity change; however, TPR measurements (11) provide no evidence for this view, and while some electronic effect due to Ru ions cannot be ruled out, a geometric explanation appears more plausible. The absence of coherent X-ray diffraction after O/LTR, when the dispersion signalled by other methods is so low that it is to be expected, strongly suggests that a highly disordered metallic phase is formed.

A short comment on the chemisorption of hydrogen on well-dispersed Ru catalysts is in order. The literature provides a number of references to the sensitivity of the process to operating variables, these showing that it is often relatively slow and that long equilibration times, aided by the use of superambient temperature, are required. The presence of impurities such as Cl^- has sometimes been blamed (30). Sticking coefficients on single-crystal Ru surfaces are high (28), and our observation (11) that hydrogen chemisorption on the very small Ru particles present in RuEC1 after HTR1 (where Cl^- is absent) is slow and not easily reproducible suggests that the process is activated. On the basis of measurements made with Ru alloys it has been thought that a minimum ensemble size of five

to nine atoms is needed for the H_2 molecule to dissociate and chemisorb (31), and even if this number is exaggerated the view is consistent with the slow chemisorption that our very small Ru clusters show. One possibility not previously canvassed is that the slow step is in fact the surface migration (spillover) of H atoms from those few particles that are sufficiently large to those that are not large enough to sustain the process. Nevertheless, chemisorption when it has taken place is strong, the isosteric enthalpy change being greater for small particles than large ones (7). In harmony with this difference, we find that the hydrogen chemisorption isotherm on RuEC3 after HTR1 shows the expected sharp change in slope and an extended plateau region, unlike that reported (11) (and recently confirmed) for RuEC1 after HTR1. The process on small Ru particles in undoubtedly complex (32) and dependent on the form of pretreatment as well as particle size.

Finally, it is necessary to contemplate the significance of the rate constants k_1 and the derived (7) true activation energies. Following the teaching of the Absolute Rate Theory, k_1 when expressed per active center will contain the intrinsic rate of conversion of the transition state into products. It would be surprising if this was not itself some function of the strength of binding of the reactants to the surface.

ACKNOWLEDGMENT

We acknowledge with thanks the financial support of the European Union under Stimulation Action Programme SC1*-CT91-0681.

REFERENCES

1. Bond, G. C., *Acc. Chem. Res.* **26**, 490 (1993); *Chem. Soc. Rev.* **20**, 441 (1991).
2. Bond, G. C., and Lou, Hui, *J. Catal.* **137**, 462 (1992).
3. Bond, G. C., and Donato, A., *J. Chem. Soc. Faraday Trans.* **89**, 3129 (1993).
4. Bond, G. C., and Xu, Yide, *J. Chem. Soc. Faraday Trans. 1* **80**, 3103 (1984).
5. Bond, G. C., Rajaram, R. R., and Burch, R., *J. Phys. Chem.* **90**, 4877 (1986).
6. Bond, G. C., and Slaa, J. C., *J. Mol. Cat. A: Chem.* **96**, 163 (1995).
7. Bond, G. C., and Slaa, J. C., *J. Mol. Cat. A: Chem.* **98**, 81 (1995).
8. Coq, B., Bittar, A., Figuéras, F., *Appl. Catal.* **59**, 103 (1990).
9. Coq, B., Bittar, A., Dutartre, R., and Figuéras, F., *J. Catal.* **128**, 275 (1991).
10. Coq, B., Crabb, E., Figuéras, F., *J. Mol. Catal. A* **96**, 35 (1995).
11. Coq, B., Crabb, E., Warawdekar, M., Bond, G. C., Slaa, J. C., Galvagno, S., Mercadante, L., García Ruiz, J., and Sanchez Sierra, M. C., *J. Mol. Catal.* **92**, 107 (1994).
12. Bond, G. C., Rajaram, R. R., and Burch, R., *in* "Proceedings, 9th International Congress on Catalysis, Calgary, 1988" (M. J. Phillips and M. Ternan, Eds.), Vol. 3, p. 1130. Chem. Institute of Canada, Ottawa, 1988.
13. Burch, R., and Paál, Z., *Appl. Catal. A* **114**, 9 (1994).
14. Kalakkad, D., Anderson, S. L., Logan, A. D., Peña, J., Braunschweig, E. J., Peden, C. F. H., and Detye, A. K., *J. Phys. Chem.* **97**, 1437 (1993).
15. Gao, S., and Schmidt, L. D., *J. Catal.* **115**, 356 (1989), and references therein.
16. Yang, C., and Goodwin, J. G., Jr., *J. Catal.* **78**, 182 (1982).
17. Sierra Sanchez, M. C., García Ruiz, J., Proietti, M. G., and Blasco, J., *J. Mol. Cat. A* **96**, 65 (1995).
18. Sierra Sanchez, M. C., Ph. D. thesis, University of Zaragoza, 1995.
19. Koningsberger, D. C., and Prins, R., "X-Ray Absorption: Principles, Applications and Techniques of EXAFS, SEXAFS and XANES." Wiley, Chichester, 1988.
20. Standards and criteria in X-ray absorption spectroscopy. *Physica B* **158**, 701 (1989).
21. Paál, Z., and Tétényi, P., *Nature (London)* **267**, 234 (1977).
22. Kempling, J. C., and Anderson, R. B., *Ind. Eng. Chem. Process Des. Dev.* **11**, 146 (1972).
23. Twizell, E. H., "Numerical Methods with Applications in the Biomedical Sciences." Ellis Horwood, Chichester, 1988.
24. Sirotti, F., Sacchi, M., Prudenziati, M., and Antonini, M., *in* "Proceedings, 2nd European Conference on Progress in X-ray Synchrotron Radiation Research" (A. Balerna, E. Berniera, and S. Mobilio, Eds.), Vol. 25, p. 547. SIF, Bologna, 1990.
25. Bond, G. C., and Gelsthorpe, M. R., *J. Chem. Soc., Faraday Trans. 1* **85**, 3767 (1989).
26. Vlaic, G., Bart, J. C. J., Cavigiolo, W., Furesi, A., Ragaini, V., Cattania Sabbadini, M. G., and Burattini, A., *J. Catal.* **107**, 263 (1987).
27. Udagawa, Y., Tohji, J., Lin, Z. Z., Okuhara, T., and Misono, M., *J. Phys. Colloq. C8* **47**, 249 (1986).
28. Lauth, G., Schwarz, E., and Christmann, K., *J. Phys. Chem.* **91**, 3729 (1989); Christmann, K., Lauth, G., and Schwarz, E., *Vacuum* **41**, 293 (1990).
29. Van Broekhoven, E. H., Schoonhoven, J. W. F. M., and Ponec, V., *Surf. Sci.* **156**, 899 (1985).
30. Bond, G. C., Rajaram, R. R., and Burch, R., *Appl. Catal.* **27**, 379 (1986); Lu, K., and Tatarchuk, B. J., *J. Catal.* **106**, 176 (1987).
31. Shimizu, H., Christmann, K., and Ertl, G., *J. Catal.* **44**, 373 (1990).
32. Bhatia, S., Engelke, F., Pruski, M., Gerstein, B. C., and King, T. S., *J. Catal.* **147**, 455 (1994).